

<https://doi.org/10.1038/s41699-026-00680-7>

Sustainable, solvent-free exfoliation of 2D materials for thermally conductive metal powder coatings



Apostolos Koutsoukis¹ ✉, Siyuan Ruan², Ruben Cabello³, Hyunjong Lee⁴, Ilias M. Oikonomou¹, Xuyun Guo¹, Arnoldas Sasnauskas², José M. Munuera^{5,6}, Aran Rafferty¹, Yifeng Xiong⁷, Sergi Dosta Parras⁶, Wessel W. Wits^{4,8}, Shuo Yin², Jonathan Coleman⁵, Rocco Lupoi² & Valeria Nicolosi¹ ✉

2D nanomaterials offer unique functional properties when combined with metal powder feedstock, enabling advanced composites for engineering and energy applications¹. Scalable fabrication of nanosheet-reinforced metal matrix composites (2DMMCs) remains challenging. In this study, we first exfoliate 2D materials using a solvent-free ball milling approach, using graphene and hexagonal boron nitride (hBN) as demonstrators, and then attach the resulting 2D nanoplatelets onto a wide range of metal powders, including copper (Cu), titanium (Ti-6Al-4V), aluminum (AlSi10Mg), and stainless steel (SS316L). To provide a mechanistic understanding of exfoliation, we use density functional theory (DFT) and discrete element method (DEM) simulations, offering new insights into the forces that drive nanosheet exfoliation. The resulting 2DMMC powders combine excellent scalability and effectiveness. After consolidation, titanium alloy/graphene systems reaching thermal conductivity values of $17 \text{ W}\cdot\text{m}^{-1}\cdot\text{K}^{-1}$, comparable or superior to previous reports. Finally, we showcase their printability, confirming compatibility with large-scale manufacturing techniques and highlighting their potential for next-generation thermal applications.

Over the past decade, 2D materials have emerged as pivotal elements of the nanotechnology revolution due to their exceptional chemical, mechanical, and electrical properties arising directly from their atomic structure^{2–5}. Their ultrathin nature allows atomic-scale control of properties, making them attractive in various technological fields. Each 2D material offers distinct advantages: graphene is an outstanding thermal and electrical conductor; hexagonal boron nitride (hBN) is an electrical insulator with excellent thermal conductivity; transition metal dichalcogenides (TMDs) such as MoS_2 and WS_2 serve as semiconductors for electronic and optoelectronic devices. The growing family of layered materials continues to expand opportunities across electronics, energy storage, and thermal management^{3,6}.

Extensive research on 2D materials has led to a plethora of various approaches for producing monolayers and a few layers of 2D nanoplatelets including liquid phase exfoliation^{7,8}, intercalation², and top-down

mechanical milling of 2D crystals⁹. Among these, mechanical ball milling stands out for its scalability and simplicity. However, it still faces important limitations.

Traditionally, the ball milling requires long processing times^{10–12} and the use of additives such as solvents (e.g., DMF¹³), polymers (e.g., melamine¹⁴), or viscous media^{15–18}. While viscous media can localize shear forces and enhance the exfoliation efficiency, they often involve complex multi-step procedures and introduce impurities that compromise the structural integrity and integration potential of the nanoplatelets. As a result, the full potential of ball milling as a scalable and sustainable technique remains underexploited. On this, we redefine the method. By optimizing energy transfer and milling dynamics, we achieve efficient exfoliation and direct coating of metal powders without any external additives^{18–20}.

Metals in parallel have a crucial role in the human progress from Bronze Age to today driving innovation and serving as vital components for

¹School of Chemistry, CRANN and AMBER Research Centres, Trinity College Dublin, Dublin, Ireland. ²Department of Mechanical Manufacturing & Biomedical Engineering, Trinity College Dublin, The University of Dublin, Dublin, Ireland. ³SDT, Departament de Ciència de Materials i Química Física, Universitat de Barcelona, Barcelona, Spain. ⁴Faculty of Electrical Engineering, Mathematics and Computer Science, University of Twente, Enschede, The Netherlands. ⁵School of Physics, CRANN & AMBER Research Centres, Trinity College Dublin, Dublin 2, Ireland. ⁶Instituto de Ciencia y Tecnología del Carbono, INCAR-CSIC, Oviedo, Spain. ⁷Centre of Excellence for Advanced Materials (CEAM), Dongguan, China. ⁸NLR—Royal Netherlands Aerospace Centre, Marknesse, The Netherlands.

✉ e-mail: koutsioa@tcd.ie; NICOLOV@tcd.ie

society²¹. Their durability under extreme conditions makes them indispensable in fields such as energy, transportation, healthcare, and infrastructure²². In additive manufacturing (AM) especially they provide high functionality and excellent formability, enabling the design of complex, lightweight, and robust components. Studies on high-entropy alloys (HEAs)²³, which combine multiple elements in equal proportions, further highlight the potential to create materials with tailored properties for next-generation applications. Together with their recyclability, metals are a game changer for sustainable technologies, addressing pressing issues such as environmental pollution and resource depletion²¹.

Combining 2D materials capabilities with metals allows the creation of composites with new properties that are otherwise impossible to achieve, unlocking advancements beyond the current limits. For example, integrating graphene or hBN into copper or titanium alloys could transform heat—dissipation strategies—a critical challenge faced by the electronics industry today²³. However, common ways to prepare such composites (molten metallurgy, powder metallurgy, or electrodeposition) face major challenges. These challenges include, low scalability, inadequate wettability and undesirable interfacial reactions^{22–26} between the 2D materials with the metal powders.

This study presents a sustainable, gram-scale strategy for coating metal powders with 2D materials. Our method starts with solvent-free ball milling exfoliation of graphite and hBN. Using density functional theory (DFT) and discrete element method (DEM) simulations, we establish a mechanistic understanding of the process. This enables uniform coverage across a wide range of metal powders, including copper, aluminum, titanium alloys, and stainless steel. The resulting 2DMMC powders display excellent thermal performance, particularly in titanium–graphene systems, and are fully compatible with additive manufacturing. After consolidation via Laser Powder Bed Fusion (LPBF), the titanium–graphene systems maintain their superior thermal properties. Overall, this approach provides a direct pathway from nanoscale engineering to scalable, real-world thermal solutions.

Results

Solvent-free exfoliation of 2D materials

To achieve uniform and defect-free coatings of metal powders with 2D materials, we developed a two-step solvent-free ball-milling strategy. In

the first step, graphite crystals are exfoliated into high-quality graphene nanoplatelets while preserving their structural integrity and mechanical flexibility. In the second step, these nanoplatelets are used to coat a variety of metal powders through a subsequent ball milling process, enabling effective attachment of the 2D phase. This solvent-free approach addresses both the challenges of producing high-quality 2D nanoplatelets and achieving uniform coverage of various metal powders without the use of solvents.

We ball-milled graphite powder for durations ranging from 2 to 48 h, using a constant ball-to-powder ratio and constant speed to control the energy input (Fig. 1a, Fig. S1). Duration of ball milling of the graphite up to 4 h results in poor dispersibility in isopropanol (IPA), whereas after 6 h, the material disperses readily in IPA, indicating the onset of exfoliation (Fig. 1d, Fig. S1a, Fig. S1d). XRD analysis of the samples support this trend, with a distinct (002) carbon peak at 26.7° emerging clearly at 6, 12, and 24 h, corresponding to highly ordered stacking of graphene nanoplatelets (Fig. 1b, Fig. S1e). A significant reduction in peak intensity at 12 h suggests substantial exfoliation and thinning into graphene nanoplatelets, while the persistence of the (002) peak indicates that the lattice remains ordered. TEM images further demonstrate the production high quality thin graphene nanoplatelets, with improved dispersibility across a range of solvents (Fig. 1f). Raman analysis and FWHM measurements reveal an I_D/I_G ratio to 0.3 (Fig. 1c), indicating low defect density and well-ordered graphene layer (Fig. S1b). Thermogravimetric analysis shows, in the case of 12 h, that the graphene nanoplatelets exhibit typical thermal behavior of graphene, with only a slight weight loss observed above 800 °C compared to graphite (Fig. S1c).

Laser diffraction particle size analysis shows a reduction in mean particle diameter $D^{3,4}$ as a function of ball-milling time, i.e., from 349 μm for graphite ball-milled for 4 h at 500 rpm, to 208 μm after 12 h, to 54 μm after 48 h (Table S1). Ball milling was also found to result in an increase in specific surface area from 1.3 $\text{m}^2 \text{g}^{-1}$ for un-ball-milled graphite to values approaching 400 $\text{m}^2 \text{g}^{-1}$ for samples milled for 48 h at 500 rpm. To assess the suitability of exfoliated nanoplatelets for metal surface attachment, we examine how morphology and surface are evolving with ball milling time. Graphite exhibited the lowest aspect ratio values, consistent with its intrinsic flake-like morphology. Upon increasing the milling duration, this

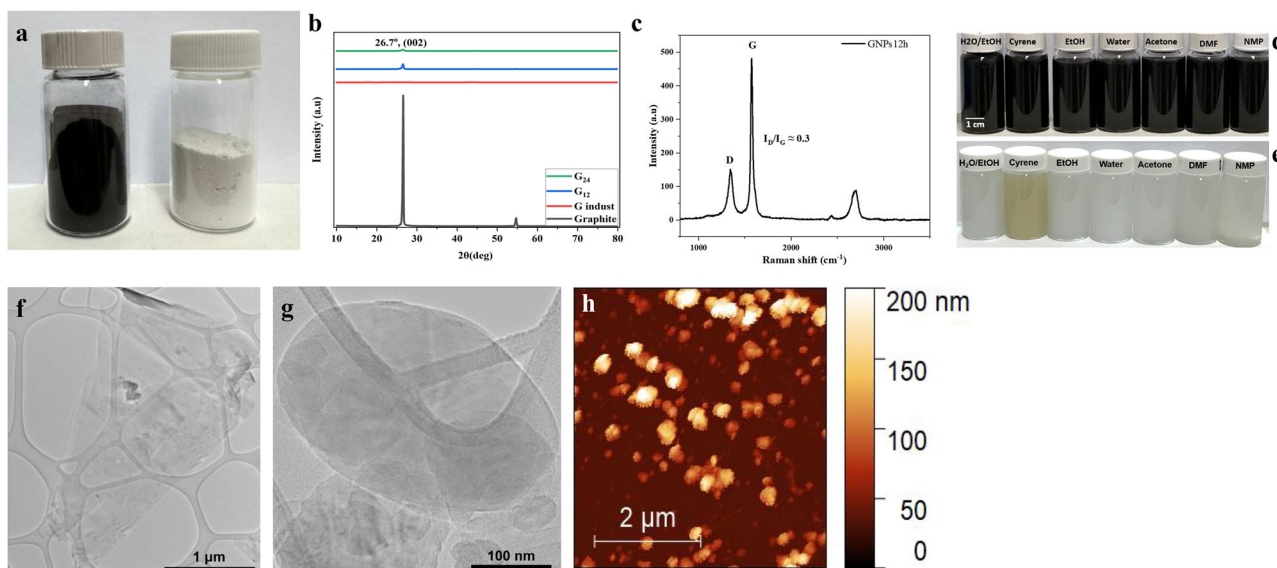
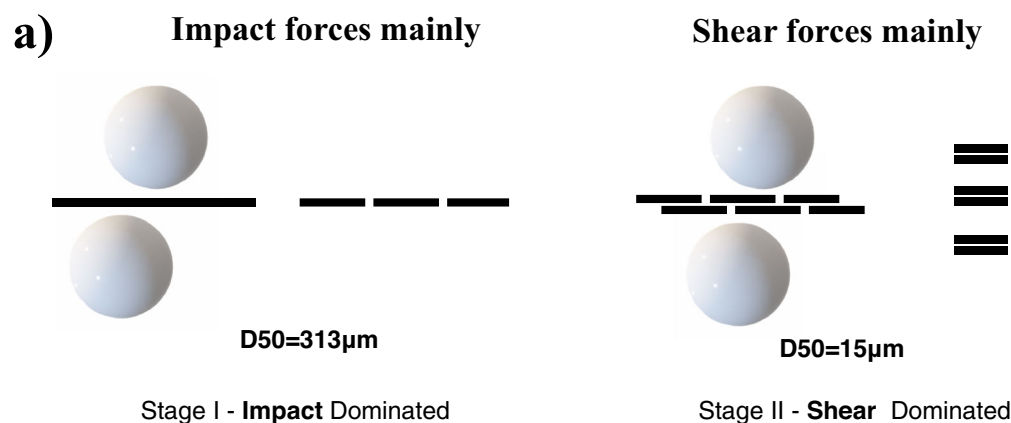


Fig. 1 | Physical and spectroscopic characterization of 2D nanoplatelets—exploring the dry ball milling technique beyond Graphene. **a** Photograph of as-produced graphene nanoplatelets (left) and the boron nitride nanoplatelets; **b** X-ray powder diffraction (XRD) patterns of pristine graphite, industrial graphene and graphene nanoplatelets after 12 and 24 h of ball milling; **c** Raman spectra of graphene

nanoplatelets at 12 h, showing the characteristic D and G bands with a low I_D/I_G ratio; **d**, **e** Dispersibility of graphene and hBN nanoplatelets at 12 h in organic solvents, water and sustainable cyrene **f** Transmission electron microscopy (TEM) image of graphene nanoplatelets at 12 h; **g** TEM image of hBN nanoplatelets at 12 h; **h** AFM image of hBN nanoplatelets at 12 h.



Shear-dominated collisions facilitate exfoliation of layered materials, enabling direct metal powder coating

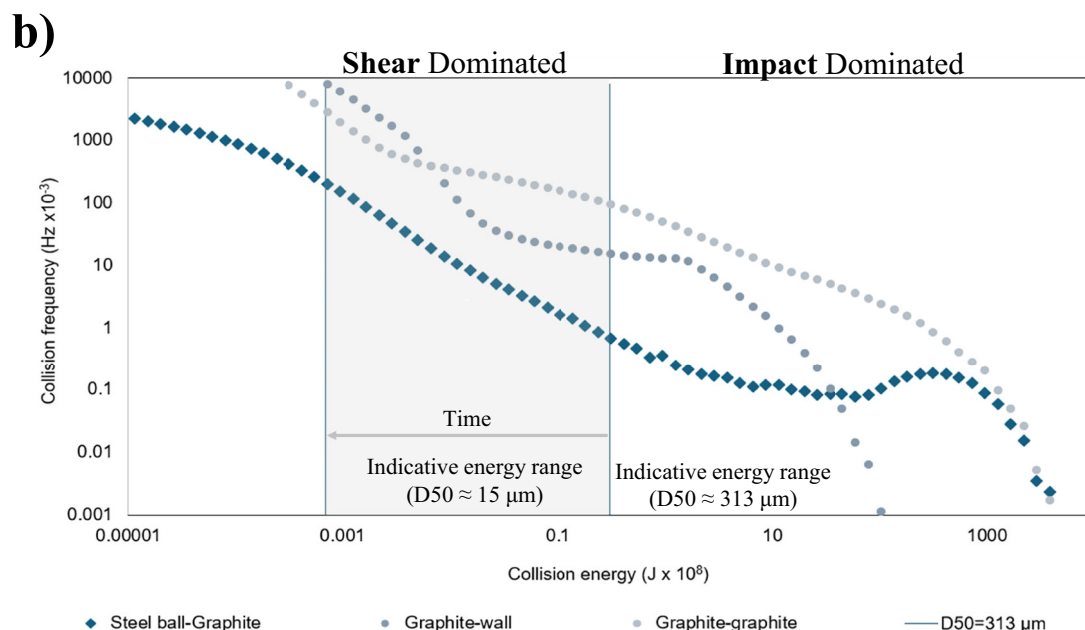


Fig. 2 | Mechanism of solvent-free ball milling exfoliation of 2D materials. **a** Schematic representation of the exfoliation mechanism during solvent-free ball milling. Early impact-dominated collisions mainly induce graphite fragmentation ($D_{50} \approx 313 \mu\text{m}$), while continued milling shifts the regime toward shear-dominated

interactions that promote layer exfoliation into thinner 2D nanoplatelets ($D_{50} \approx 15 \mu\text{m}$); **b** DEM-simulated collision energy–frequency distributions at 500 rpm, showing an increasing contribution of shear-dominated collisions above the exfoliation threshold as particle size decreases.

morphological evolution correlated with higher surface area, indicating the shape regularity enhances the accessible surface. Notably, while the average particle diameter remained relatively constant, prolonged milling led to the formation of more spherical particles.

To understand the mechanism behind solvent-free exfoliation of graphite, we focus on identifying critical stages of the exfoliation process without the use of polymers or high-viscosity solvents. Our results showcase that the fragmentation of graphite plays a dual role: it increases the surface area while lowering the energy barrier for exfoliation. A combined experimental and simulation approach—including Density Functional Theory (DFT) calculations of exfoliation energy and Discrete Element Method (DEM) modeling of ball-milling dynamics—shows that as particle size decreases under controlled milling speeds, the exfoliation process becomes more energy efficient. This indicates that solvent-free ball milling can achieve effective exfoliation by optimizing mechanical fragmentation and shear transfer to the target materials, offering a simpler and scalable route for graphene nanoplatelets production.

Mechanism of solvent-free exfoliation of 2D materials

DFT calculations confirm that exfoliating graphene layers requires $\sim 0.4 \text{ J/m}^2$ ^{27,28}. In our approach, we reduce the graphite size from $D_{50} = 313 \mu\text{m}$ to $15 \mu\text{m}$ at 500 rpm. This reduction creates a regime where exfoliation energy was significantly lowered. By reducing the particle size, the collisions occur with an energy that is better suited for exfoliation. As a result, the overall exfoliation energy is significantly reduced. At $15 \mu\text{m}$, only $\sim 7 \times 10^{11} \text{ J}$ per shear was required, with $\sim 8 \times 10^7$ such events occurring every second. In contrast, the starting graphite at $313 \mu\text{m}$ experienced only $\sim 1.5 \times 10^4$ effective collisions per second. This dramatic shift highlights how controlled fragmentation increases collision frequency and reduces the exfoliation energy barrier. At lower speeds (e.g., 150 rpm), both fragmentation and exfoliation are both delayed. At $15 \mu\text{m}$, the energy required for each shear significantly slower reduction in particle size and a longer period needed to initiate exfoliation (Fig. 2a).

DEM simulations further support our findings by showing that, at 500 rpm the collision energies generated from shear interactions are

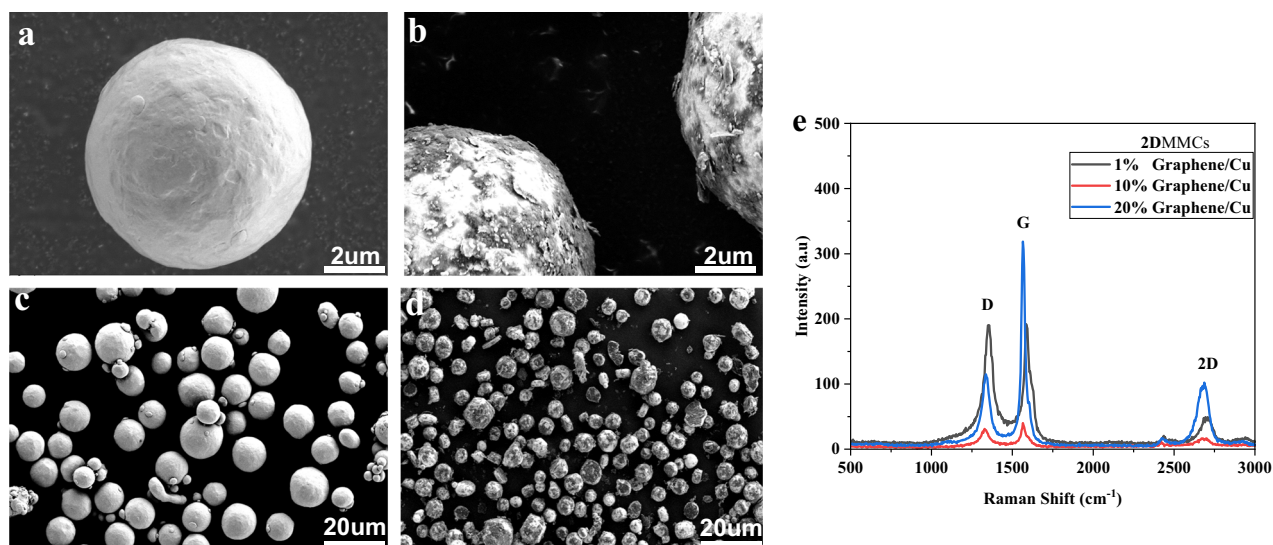


Fig. 3 | Graphene coating of Cu metal particle. **a**, **c** pure copper particle; **b**, **d** Graphene/Cu 2DMMC composite and **e** Raman spectra of Graphene/Cu 2DMMCs at different concentrations 1 wt%, 10 wt%, 20 wt%.

sufficient to promote exfoliation of the graphite crystals. According to (Fig. 2b), the number of the collision above the exfoliation threshold increased steadily as particle size decreased. Together, these results demonstrate a sustainable, scalable route to exfoliate 2D materials, suitable to coat metal powders²⁹. The DEM simulations adopt a simplified framework and do not explicitly account for van der Waals interactions or possible re-agglomeration of exfoliated nanoplatelets, which constitutes a known limitation of the model. Nevertheless, the simulations capture the dominant collision regimes governing exfoliation and are consistent with the experimentally observed behaviors.

To test the versatility of our approach, we applied the same parameters from the two-step strategy to hBN (Fig. 1e, Fig. S2)^{30–33}. TEM analysis confirmed the layered structure (Fig. 1g), while XRD showed a peak at 26.96° (002) in both bulk hBN and the exfoliated nanoplatelets, indicating that the crystal structure is preserved (Fig. S2a, S2c, d). Raman spectra exhibited a peak at 1369 cm^{-1} , slightly shifted compared to unexfoliated hBN, further supporting successful exfoliation (Fig. S2b). Finally, AFM analysis of ball-milled hBN nanoplatelets revealed an average thickness of about 13 layers, demonstrating the robustness of our solvent-free milling approach (Fig. 1h).

According to the previous studies, as the thickness of graphite or hBN decreases, the nanoplatelets show enhanced mechanical compliance and surface energy^{34,35}. In this direction, our method enables the uniform coating of a broad range of metal powders, including copper, titanium and aluminum alloys, as well as stainless steels^{32–36}.

Attachment of 2D nanoplatelets on metal particles (2DMMCs)

For the attachment of 2D nanoplatelets on the metal surfaces, we follow a mild solvent-free approach (150 rpm, 6 h) starting with copper particles and varying graphene nanoplatelets loadings (from 1 wt% to 20 wt%). SEM images of Cu/graphene 2DMMCs reveal successful surface coverage of graphene even at low content (Fig. 3a–d). Raman spectroscopy further identifies characteristic graphene peaks, providing insights into the successful coverage of the metal particle (Fig. 3e). EBSD on the pure copper before and after ball milling shows grain refinement without compromising the powder's suitability. Misorientation mapping further indicates low and stable internal stress levels, validating the mild milling conditions for effective metal surface coverage³⁷ (Fig. S3).

Cross-section analysis was performed on graphene/copper and graphene/titanium-alloy 2DMMCs composites to investigate the graphene distribution on the metal particle surface. (Fig. 4a–c) show a representative HAADF-STEM image of a graphene/copper composite particle; the overlay

in (Fig. 4c) showcases the corresponding energy loss spectroscopy (EELS) maps, showcasing the presence of copper (red), carbon (blue), and oxygen (green) layers, and confirming the uniform distribution of graphene around the copper particle. The same type of characterization follows on graphene/titanium alloy composites (Fig. 4d–f), confirming the uniform distribution of graphene around the titanium alloy particle. Both material systems exhibit smooth and continuous interfaces without significant voids or gaps, indicating robust interfacial mechanical bonding between the graphene nanoplatelets and the metal powder surface. Cross-sectional characterization of copper and titanium alloy 2DMMCs using TEM, HRTEM and SAED, further confirms the presence of a graphene layer on the metal surface for both titanium alloy and copper particles (Fig. S4–S5). Based on this mechanical bonding^{38,39}, primarily driven by van der Waals interactions between the graphene (2D material) and metal particle, we demonstrate further that the thickness of the coating layer on the metal particles can be tailored and significantly increased from the nanoscale (120–320 nm) to the microscale (~ 1.2 – $1.8\ \mu\text{m}$), as shown in Fig. S6.

Scalability and thermal performance of 2DMMCs

After confirming the coverage of copper and titanium particles with graphene nanoplatelets, we extend our approach to a broad range of metal powders from stainless steel (SS316L), Ti6Al4V and AlSi10Mg alloys with both graphene and hBN. SEM images confirm seamless attachment of 2D nanoplatelets across all metals, showing robust and uniform coverage of the 2D phase. Further, this strategy on 2DMMCs shows great potential for scalability: we demonstrate this by increasing graphene production in our small-scale laboratory starting from 8 to 24 g of graphene in 24 h, with similar results for hBN nanoplatelets (Fig. S7). Similarly, we can upscale the production of the 2DMMCs composites from 1 g after 6 h of solvent-free ball milling to 480 g after 24 h following the same ball-to-powder ratio of small-scale production (Fig. S8). Beyond the industrial scale potential of our approach, the consolidated titanium alloy/graphene composites at this level exhibit significant thermal enhancements (Fig. 5).

Graphene-coated titanium alloy powders were consolidated using spark plasma sintering (SPS), resulting in dense and uniform composites. The conformal graphene coverage prior to sintering ensured homogeneous carbon distribution, which is critical for the formation of efficient thermal transport pathways^{40,41}. At 10 wt% graphene, the composites reached a thermal conductivity of $17\text{ W}\cdot\text{m}^{-1}\cdot\text{K}^{-1}$, approximately 2.5 times higher than that of uncoated Ti-6Al-4V ($6.65\text{ W}\cdot\text{m}^{-1}\cdot\text{K}^{-1}$) (Table S2). XRD analysis indicates the formation of strong Ti-C interfacial interactions, evidenced by reflections in the 36 – 42° range (Fig. 5a), which are consistent with the

Fig. 4 | Cross-sectional characterization of graphene-coated metal powders (2DMMCs). a-c **Graphene/Cu 2DMMC**; a cross-sectional SEM image of a single Cu particle b HAADF-STEM image highlighting continuous graphene nanoplatelets surface layer (green dashed box), and c HAADF-STEM image and corresponding EELS maps of Graphene/Cu 2DMMC d-f **Graphene/Titanium alloy 2DMMC**; d cross-sectional SEM image of a Ti alloy particle, e HAADF-STEM image showing graphene nanoplatelets-containing surface layer (green dashed box), and f HAADF-STEM image and corresponding EELS maps of Graphene/Titanium alloy 2DMMC.

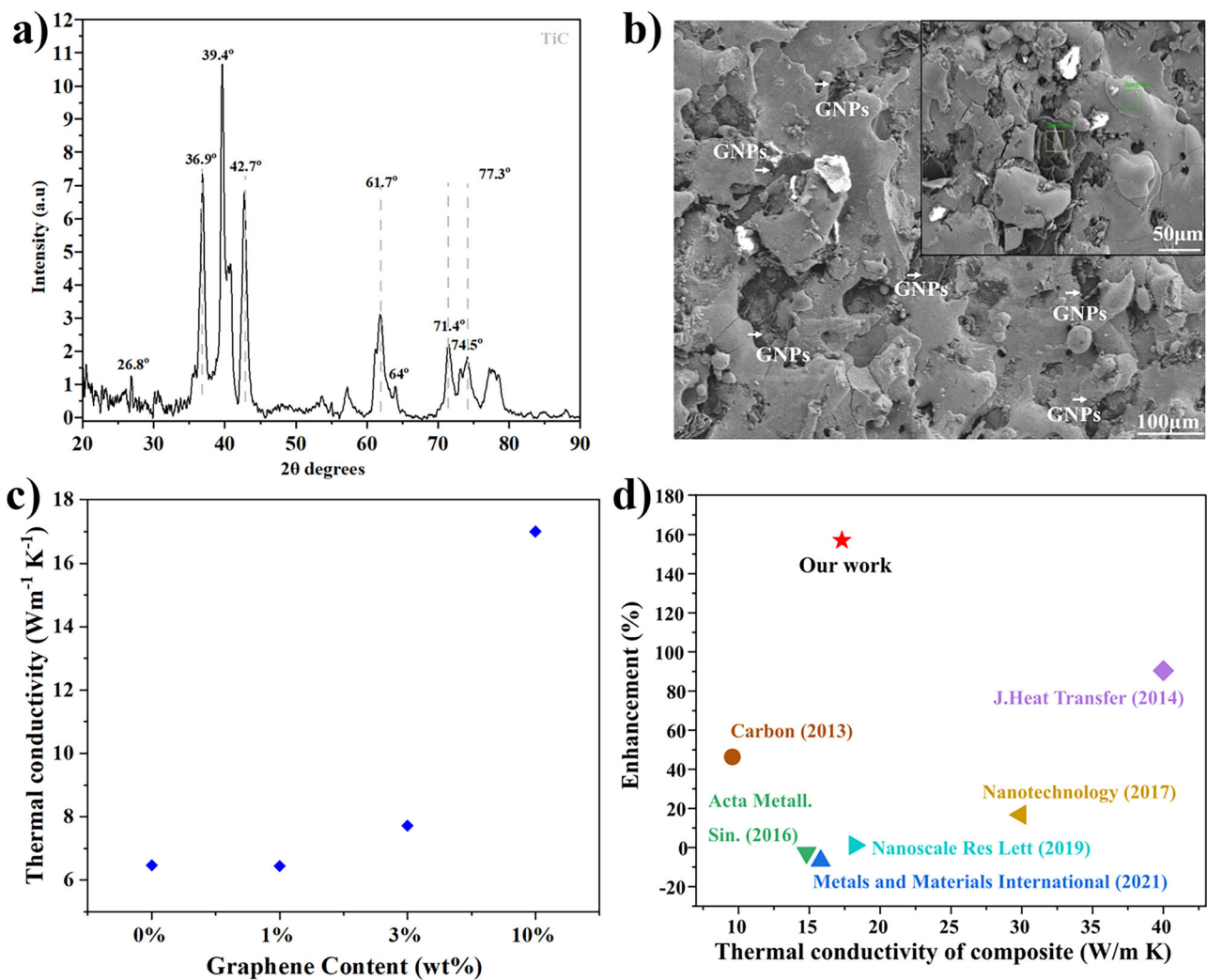
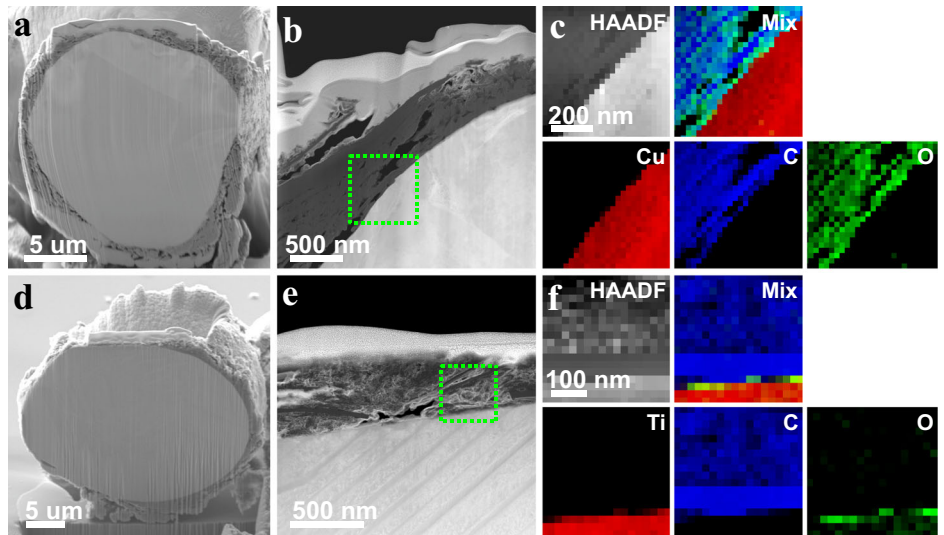


Fig. 5 | Thermal performance of 2DMMCs. a XRD pattern of the Ti alloy reinforced with 10 wt% graphene. XRD pattern of the consolidated Ti-graphene composite showing the characteristic TiC peak, confirming interfacial reactions during sintering. The pattern is lightly smoothed using a Savitzky-Golay filter (20 points) for clarity b SEM micrograph revealing a homogeneous distribution of graphene nanoplatelets within the titanium alloy matrix (inset: higher-magnification image

highlighting embedded GNPs) c Thermal conductivity enhancement of Graphene/Ti alloy 2DMMCs as a function of graphene content (wt%) d Comparison of thermal conductivity enhancement versus thermal conductivity of composite materials reported in the literature, highlighting the performance of the present work (red star).

formation of carbide-like bonding at the graphene–titanium alloy interface during SPS processing. Given that the intrinsic thermal conductivity of Ti-6Al-4V (Fig. 5b), is approximately $6.65 \text{ W}\cdot\text{m}^{-1}\cdot\text{K}^{-1}$, the significantly higher value obtained here indicates an additional bulk contribution arising from the incorporation of graphene nanoplatelets and the formation of thermally conductive networks within the matrix (Fig. 5c). To the best of our knowledge^{42–49}, the thermal conductivity values reported here rank among the highest for graphene/titanium composites produced by scalable methods (Fig. 5d), confirming the effectiveness of graphene incorporation and Ti-C interfacial interactions in enhancing thermal transport (Table S3).

LPBF printability of 2DMMCs for additive manufacturing

Finally, to integrate our 2DMMCs platform with large-scale manufacturing techniques, we demonstrate their printability using the LPBF technique. LPBF is a powerful additive manufacturing technique, enabling the creation of freeform geometries, complex features, and tool-less fabrication, with high resolution and excellent surface quality. Starting from titanium alloy composites with graphene or hBN nanoplatelets, as well as stainless steel 316 L with graphene, we achieved successful deposition of the 2D phase through metal melting, even at low nanosheet loadings. Raman spectroscopy of the printed parts confirmed the retention of graphene characteristics, with an I_D/I_G ratio of 0.34, close to the initial nanoplatelets (Fig. S9). The 2D coverage of the metal particles facilitates high-quality, uniform printed structures, according to RAMAN and SEM, which revealed the presence of carbon from the graphene nanoplatelets compared to pure titanium (Figs. S10, S11). While further studies are needed to expand the material scope, these results underscore the robustness and versatility of our solvent-free approach for producing thermally enhanced, high-performance, and printable 2DMMCs.

Discussion

We demonstrate a sustainable and scalable method to produce 2D metal matrix composites (2DMMCs) via solvent-free ball milling, coating copper, titanium (Ti-6Al-4V), aluminum (AlSi10Mg) alloys, and stainless steel (SS316L) powders with 2D nanoplatelets. This approach avoids so high viscous solvents or surfactants and is compatible with industrial-scale manufacturing. For the exfoliation of 2D materials we conclude with a mechanistic insight from DFT and DEM simulations reveals optimal energy transfer and particle collision dynamics that reduce the interlayer energy barrier. For $15 \mu\text{m}$ particles, only $\sim 7 \times 10^{11} \text{ J}$ per shear is needed, with $\sim 8 \times 10^7$ events per second over a thousand times more than the $\sim 1.5 \times 10^4$ effective collisions at $313 \mu\text{m}$. We scale up the 2DMMCs platform, achieving titanium-based composites with significantly enhanced thermal conductivity ($17 \text{ W m}^{-1} \text{ K}^{-1}$ at 10 wt% graphene), attributed to newly formed carbon–titanium bonds. These composites are also fully printable via the LPBF technique. Finally, while this study focused primarily on the preparation of 2DMMCs for thermal management applications, preliminary observations suggest excellent promise in the energy field as well.

Methods

Materials

Graphite (Graphite, 332461 Sigma-Aldrich). Boron nitride (boron nitride, 2555476, Sigma-Aldrich), Copper powder ($-38 + 15 \mu\text{m}$, Safina), AlSi₁₀Mg (PowderRange—Carpenter Additive, 20–63 μm), Ti64Al4V (Powder Range—Carpenter Additive, 15–53 μm), Steel 316 L (Powder Range – Carpenter Additive, 15–45 μm).

Preparation of 2DMMCs

In a typical experiment, 1 g of graphite flakes was mixed in milling jars (two to four mostly) under an argon atmosphere (Ag) and milled at 500 rpm for 2–48 h, with a powder-to-balls ratio: 1 to 20 (steel balls, 0.5 mm diameter) and each of the ball-milled graphene nanoplatelets was collected as G_x ($x = 2, 6, 12, 24, 48 \text{ h}$). We followed the same procedure for the preparation of for few layer hBN nanoplatelets using the best conditions from the graphene method, mentioning this product as hBN_x. For

the large-scale production of graphene, we used the same ration of balls to powder with a mass of starting graphite of 3 g for each jar. After the end of the process, the 2D phase is used for the preparation of 2DMMCs. A further step of preparing 2DMMCs is followed up, by mixing the graphene or hBN nanoplatelets with metal powder (different mass ratios), a ratio of powder to balls, 1 to 10, under argon atmosphere for 6 h at 150 rpm. This method can apply to different metal powder of copper, AlSi₁₀Mg, steel 316 L, and Ti64Al4V. The large scalability of this method can be expanded for 30 g of the 2DMMCs composites (two to four mostly) with the same ratio of the balls to powder 1 to 10, at 150 rpm 6 h (in total 120 g of preparation at 6 h).

Characterization of 2DMMCs

Scanning electron microscopy (SEM) was conducted using the Zeiss ULTRA plus Gemini SEM microscope in high vacuum mode with an acceleration voltage of 5 kV, a working distance of 6 mm, and a 30 μm aperture located in the Advanced Microscopy Laboratory (AML) of TCD.

Transmission electron microscopy (TEM) was performed using uncorrected FEI Titan with Schottky field emission S-FEG source operated at 300 kV. TEM images were recorded using a Gatan UltraScan CCD camera and electron energy-loss spectroscopy (EELS) mapping was carried out with Quantum Gatan Imaging Filter (GIF) detector with energy dispersion of 0.5 eV per channel.

Ball milling machine PQ-N2 500 mL \times 4 planetary 220 V PQN2.220–50 Hz. X-ray diffraction (XRD) measurements were performed using a Panalytical X'Pert Pro-diffractometer with a Cu K α source ($\lambda = 1.5406 \text{ \AA}$). Symmetric scans run over a 2θ range of 10° to 75° , with a step size of 0.0084° .

Raman spectroscopy performed using a WITec Alpha 300 R with 532 and 633 nm excitation lasers with a spectral grating of 1800 lines/mm and a $100\times$ microscope aim (0.95 N.A., spot size $\sim 0.3 \mu\text{m}$). Spectra taken with a laser power of $<300 \mu\text{W}$ in order to minimize sample heating.

Thermogravimetric analysis (TGA) was conducted from 50 to 900°C with the temperature rising rate of $10^\circ\text{C}/\text{min}$ under continuous nitrogen flow (PerkinElmer TGA 8000).

Particle Size Distribution Malvern Mastersizer 2000 (Model APA2000) Malvern Instruments Ltd., UK.

Thermal conductivity measurements graphene/Ti Alloy 2DMMCs

For the thermal characterization of SPS Graphene/Ti alloy 2DMMCs, we utilized the transient plane source (TPS) technique to measure their thermal conductivity⁵⁰. TPS methodology was selected as it enables characterization of samples with various geometries, including slabs, rods, and bulk disks.

Accordingly, a cylindrical slab geometry with a high aspect ratio of diameter to thickness was chosen to ensure the in-plane thermal conductivity measurements of 2DMMCs, by geometrically confining the predominant radial-directed heat flow compared to axial direction⁵¹.

Specifically, slabs with a diameter of 30 mm and a thickness of 1 mm are prepared using a wire electrical discharge machining tool (CUT AM 500, GF Machining Solutions, Switzerland), equipped with a 0.2 mm thick pure Mo wire.

The reproducibility and reliability of measurements were secured by conducting three repeated tests for each set. Each set is composed of two slabs sandwiching a 6.4mm-sized double-sided sensor (MP-1 two-sided sensors, Thermtest, Canada), measuring a total of three slabs.

As a result, these testing method enables the measurement of more than half of the entire SPS cylinder (30 mm diameter and 5–6 mm thickness), representing the overall thermal properties of Ti alloy-graphene 2DMMCs.

Data availability

All the data generated or analyzed during this study are included in this published article and its supplementary file.

Received: 6 October 2025; Accepted: 9 February 2026;

Published online: 18 February 2026

References

- Miracle, D. Metal matrix composites from science to technological significance. *Compos. Sci. Technol.* **65**, 2526–2540 (2005).
- Nicolosi, V. et al. Liquid exfoliation of layered materials. *Science* **340**, 1226419 (2013).
- Pham, P. V. et al. 2D heterostructures for ubiquitous electronics and optoelectronics: principles, opportunities, and challenges. *Chem. Rev.* **122**, 6514–6613 (2022).
- Pham, P. V. et al. Layer-by-layer thinning of two-dimensional materials. *Chem. Soc. Rev.* **53**, 5190–5226 (2024).
- Pham, P. V. et al. Transfer of 2D films: from imperfection to perfection. *ACS Nano* **18**, 14841–14876 (2024).
- Coleman, J. N. et al. Two-dimensional nanosheets produced by liquid exfoliation of layered materials. *Science* **331**, 568–571 (2011).
- Hernandez, Y. et al. High-yield production of graphene by liquid-phase exfoliation of graphite. *Nat. Nanotechnol.* **3**, 563–568 (2008).
- Koutsoukis, A. et al. Stable dispersion of graphene in water, promoted by high-yield, scalable exfoliation of graphite in natural aqueous extracts: the role of hydrophobic organic molecules. *ACS Sustain. Chem. Eng.* **10**, 12552 (2022).
- Lyu, H. et al. Ball-milled carbon nanomaterials for energy and environmental applications. *ACS Sustain. Chem. Eng.* **5**, 9568–9585 (2017). 11.
- Welham, N. J., Berbenni, V. & Chapman, P. G. Effect of extended ball milling on graphite. *J. Alloy. Compd.* **349**, 255–263 (2003).
- Jeon, I.-Y. et al. Edge-carboxylated graphene nanosheets via ball milling. *Proc. Natl. Acad. Sci. USA* **109**, 5588–5593 (2012).
- Xing, T. et al. Disorder in ball-milled graphite revealed by Raman spectroscopy. *Carbon* **57**, 515–519 (2013).
- Zhao, W. et al. Preparation of graphene by exfoliation of graphite using wet ball milling. *J. Mater. Chem.* **20**, 5817–5819 (2010).
- León, V. et al. Few-layer graphenes from ball-milling of graphite with melamine. *Chem. Commun.* **47**, 10936–10938 (2011).
- Yang, L. et al. Glue-assisted grinding exfoliation of large-size 2D materials. *Mater. Today* **51**, 145–154 (2021).
- Shi, D. et al. Ultrasonic-ball milling: a novel strategy to prepare large-size ultrathin 2D materials. *Small* **16**, 1906734 (2020).
- Zhou, Y. et al. Viscous solvent-assisted planetary ball milling for the scalable production of large ultrathin two-dimensional materials. *ACS Nano* **16**, 10179–10187 (2022).
- Wang, Z. et al. Scalable high-yield exfoliation for monolayer nanosheets. *Nat. Commun.* **14**, 236 (2023).
- Liu, X. Ingang et al. A review on mechanochemistry: approaching advanced energy materials with greener force. *Adv. Mater.* **34**, 210832 (2022).
- Raabe, D. The materials science behind sustainable metals and alloys. *Chem. Rev.* **123**, 2436–2608 (2023).
- Raabe, D., Tasan, C. C. & Olivetti, E. A. Strategies for sustainable metals production. *Nature* **575**, 64–74 (2019).
- George, E. P., Raabe, D. & Ritchie, R. O. High-entropy alloys. *Nat. Rev. Mater.* **4**, 515–534 (2019).
- Wang, H. et al. Thermal transfer in graphene-interfaced materials: contact resistance and interface engineering. *ACS Appl. Mater. Interfaces* **5**, 2599–2603 (2013). 7.
- Chen, D. et al. Graphene-reinforced metal matrix composites: fabrication, properties, and challenges. *Int. J. Adv. Manuf. Technol.* **125**, 2925–2965 (2023).
- Mussatto, A., Ahad, I. U., Mousavian, R. T., Delaure, Y. & Brabazon, D. *Eng. Rep.* **3**, e12330 (2021).
- Mussatto, A. et al. Advanced production routes for metal matrix composites. *Eng. Rep.* **3**, 12330 (2020).
- Sharma Kumar, D., Mahant, D. & Upadhyay, G. Manufacturing of metal matrix composites: a state of review. *Mater. Today.: Proc.* **26**, 506–519 (2020).
- Wang, W. et al. Measurement of the cleavage energy of graphite. *Nat. Commun.* **6**, 7853 (2015).
- Jung, J. H., Park, C. H. & Ihm, J. A rigorous method of calculating exfoliation energies from first principles. *Nano Lett.* **18**, 2759–2765 (2018).
- Gou, D. et al. DEM modelling of particle fragmentation during compaction of particles. *Powder Technol.* **398**, 117073 (2022).
- Naclerio, A. E. & Kidambi, P. R. A review of scalable hexagonal boron nitride (h-BN) synthesis for present and future applications. *Adv. Mater.* **35**, 2207374 (2023).
- Huang, C. et al. Stable colloidal boron nitride nanosheet dispersion and its potential application in catalysis. *J. Mater. Chem. A* **1**, 12192–12197 (2013).
- Ghosh, A. et al. Liquid exfoliation of hexagonal boron nitride. *J. Mater. Eng. Perform.* **33**, 5364–5379 (2024).
- Singh, B. et al. Nanostructured boron nitride with high water dispersibility for boron neutron capture therapy. *Sci. Rep.* **6**, 35535 (2016).
- Eledath, A. N., Poullose, A. E. & Muthukrishnan, A. Synthesis of few-layer graphene by ball-milling for oxygen reduction: kinetics and mechanistic insights. *ACS Appl. Eng. Mater.* **1**, 2304–2314 (2023).
- Blees, M. K. et al. Graphene kirigami. *Nature* **524**, 204–207 (2015).
- Dontsova, E. & Traian, D. Nanomechanics of twisted mono- and few-layer graphene nanoribbons. *J. Phys. Chem. Lett.* **4**, 2010–2014 (2013).
- Wei, Y. et al. Bending rigidity and Gaussian bending stiffness of single-layered graphene. *Nano Lett.* **13**, 26–30 (2013).
- Hu, T. et al. Quantifying the rigidity of 2D carbides (MXenes). *Phys. Chem. Chem. Phys.* **22**, 2115–2121 (2020).
- Suryanarayana, C. Mechanical alloying and milling. *Prog. Mater. Sci.* **46**, 1–184 (2001).
- Benjamin, J. S. & Volin, T. E. The mechanism of mechanical alloying. *Metall. Trans.* **5**, 1929–1934 (1974).
- Lee, H. et al. Review on properties, physics, and fabrication of two-dimensional material-based metal-matrix composites (2DMMCs) for heat transfer systems. *Renew. Sust. Energy Rev.* **217**, 115700 (2025).
- Lee, H. et al. Characterization of thermal properties of ball-milled copper-graphene powder as feedstock for additive manufacturing. *Powder Technol.* 121423 (2025).
- Yan, Q. et al. Simultaneously improving mechanical, thermal, and anti-wear properties of Ti alloys using 3D-networked graphene as reinforcement. *Carbon* **213**, 118152 (2023).
- Gürbüz, M., Tuğba, M. & Pinar, U. Mechanical, wear and thermal behaviors of graphene reinforced titanium composites. *Met. Mater. Int.* **27**, 744–752 (2021).
- Yang, W.-Z. et al. Thermal and mechanical properties of graphene-titanium composites synthesized by microwave sintering. *Acta Metall. Sin. (Engl. Lett.)* **29**, 707–713 (2016).
- Zheng, H. & Jaganandham, K. Thermal conductivity and interface thermal conductance in composites of titanium with graphene platelets. *J. Heat. Transf.* **136**, 061301 (2014).
- Wang, J. et al. Electrochemical depositing rGO-Ti-rGO heterogeneous substrates with higher thermal conductivity and heat transfer performance compared to pure Ti. *Nanotechnology* **28**, 075703 (2017).
- Liu, J. et al. Microstructure and mechanical properties of graphene oxide-reinforced titanium matrix composites synthesized by hot-pressed sintering. *Nanoscale Res. Lett.* **14**, 114 (2019).
- Gustafsson, S. E. Transient plane source techniques for thermal conductivity and thermal diffusivity measurements of solid materials. *Rev. Sci. Instrum.* **62**, 797–804 (1991).
- Gustavsson, M., Karawacki, E. & Gustafsson, S. E. Thermal conductivity, thermal diffusivity, and specific heat of thin samples

from transient measurements with hot disk sensors. *Rev. Sci. Instrum.* **65**, 3856–3859 (1994).

Acknowledgements

V.N. wishes to thank the support of the SFI-funded AMBER research center, and the SFI Frontiers for the Future award (Grant Nos. 12/RC/2278_P2 and 20/FFP-A/8950, respectively). Furthermore, V.N. and A.K. wish to thank the support of the EIC Pathfinder ThermoDust project (project number 101046835). I.M.O. and V.N. acknowledge support from the European Union's Horizon 2020 research and innovation program under Agreement No. 956813. S.R., R.L. and S.Y. acknowledge support from the EIC Pathfinder ThermoDust project (Project No. 101046835). A.S. acknowledges support from Science Foundation Ireland (18/EPSC-CDT/3581) and the Engineering and Physical Sciences Research Council (EP/S023259/1). J.M.M. thanks the Spanish Government's Generation D initiative, promoted by Red.es, an organization attached to the Ministry for Digital Transformation and the Civil Service, for the attraction and retention of talent through grants and training contracts, financed by the Recovery, Transformation and Resilience Plan through the European Union's Next Generation funds. Furthermore, V.N. and X.G. wish to thank the Advanced Microscopy Laboratory (AML) in CRANN for the provision of their facilities and thank Clive Downing for optimizing the microscope.

Author contributions

R.L. and V.N. conceived and supervised the overall project. A.K. designed and performed the experiments, analyzed the data, interpreted the results, and drafted the manuscript. S.R. assisted with ball milling experiments and data analysis. R.C. and S.D.P. developed and executed the computational model supporting the experimental work. I.M.O. and X.G. performed TEM characterization and analyzed the corresponding data. A.R. performed materials characterization, including measurements of the surface energy and particle size distribution, and Y.X. carried out the SPS methodology. A.S. conducted BSD measurements. J.M.M. performed AFM measurements. H.L. and W.W.W. performed thermal conductivity measurements and contributed to their interpretation. J.C. and S.Y. contributed to discussions on experimental design and results. All authors contributed to writing, reviewed, and corrected the final manuscript, and approved its submission.

Competing interests

The authors declare no competing interests. V.N. is an Associate Editor of *npj 2D Materials and Applications* but was not involved in the peer review of this article and had no access to information regarding its peer review. Full responsibility for the editorial process for this article was delegated to another journal editor.

Additional information

Supplementary information The online version contains supplementary material available at <https://doi.org/10.1038/s41699-026-00680-7>.

Correspondence and requests for materials should be addressed to Apostolos Koutsoukis or Valeria Nicolosi.

Reprints and permissions information is available at <http://www.nature.com/reprints>

Publisher's note Springer Nature remains neutral with regard to jurisdictional claims in published maps and institutional affiliations.

Open Access This article is licensed under a Creative Commons Attribution 4.0 International License, which permits use, sharing, adaptation, distribution and reproduction in any medium or format, as long as you give appropriate credit to the original author(s) and the source, provide a link to the Creative Commons licence, and indicate if changes were made. The images or other third party material in this article are included in the article's Creative Commons licence, unless indicated otherwise in a credit line to the material. If material is not included in the article's Creative Commons licence and your intended use is not permitted by statutory regulation or exceeds the permitted use, you will need to obtain permission directly from the copyright holder. To view a copy of this licence, visit <http://creativecommons.org/licenses/by/4.0/>.

© The Author(s) 2026